

Gravitational Wave Effects on Radio Spectral Lines of Atomic Hydrogen: Hyperfine Splitting and Broadening Mechanisms

Nontapat Wanwieng*

National Astronomical Research Institute of Thailand (NARIT), Chiang Mai, 50180, Thailand

Nithiwadee Thaicharoen and Narupon Chattapiban

*Department of Physics and Materials Science, Faculty of Science,
Chiang Mai University, Chiang Mai 50200, Thailand*

Apimook Watcharangkool†

*National Astronomical Research Institute of Thailand (NARIT), Chiang Mai, 50180, Thailand and
Department of Physics and Materials Science, Faculty of Science,
Chiang Mai University, Chiang Mai 50200, Thailand*

(Dated: March 18, 2025)

We explore the effects of gravitational waves (GWs) on hydrogen's radio spectral lines, focusing on the ground-state hyperfine transition and radiative transitions in highly excited Rydberg states. To analyze GW impacts on hyperfine structure, we derive Maxwell's equations in a gravitational-wave background using linearized gravity and the $3 + 1$ formalism. Our findings reveal that GWs induce energy shifts in hyperfine magnetic substates, modifying the 21 cm line. However, these energy shifts fall well below the detection limits of current radio astronomical instruments. For transitions in highly excited states, which produce radio recombination lines (RRL), the influence of GW manifests itself as spectral broadening, with the fractional linewidth for $Hn\alpha$ scaling as $\Delta\nu/\nu_0 \sim n^7 \omega_{\text{gw}}^2 h(t)$. This suggests that RRLs could serve as probes for ultra-high-frequency GWs, particularly given that Rydberg atoms in the interstellar medium can reach quantum numbers above $n = 100$. As an example of possibly detectable high frequency GW source, We investigate GWs emitted during the inspiral of planetary-mass primordial black hole binaries, where GW-induced broadening in RRLs could exceed natural broadening effects. Additionally, we examine the influence of the recently detected stochastic gravitational-wave background on hydrogen spectral lines.

Keywords: Gravitational wave, Atomic hydrogen, Hyperfine structure, Radio recombination lines, Electrodynamics in curved spacetime, Linearized gravity, Spectral broadening

I. INTRODUCTION

Gravitational waves (GWs), as predicted by Einstein's General Relativity [1, 2], are ripples in spacetime that travel at the speed of light. Since their first direct detection by LIGO in 2015 [3], GWs have provided unprecedented insights into astrophysical phenomena that were previously inaccessible through traditional electromagnetic observations. More recently, the detection of a stochastic gravitational-wave background (SGWB) by Pulsar Timing Arrays (PTAs) [4] has expanded our ability to probe the universe on cosmological scales.

GWs cover a broad range of frequencies, each linked to specific astrophysical sources and detection techniques. Nanohertz-frequency GWs are monitored by PTAs, which primarily detect signals from supermassive black hole binaries. The space-based LISA mission will observe the millihertz band, detecting compact binary systems such as white dwarf mergers and extreme-mass-ratio inspirals. Ground-based detectors like LIGO, Virgo, and KAGRA operate in the tens of hertz to several kilohertz range, capturing mergers of stellar-mass black holes

and neutron stars. Meanwhile, GWs above 10 kHz remain largely uncharted but could provide insights into exotic sources such as primordial black holes or physics beyond the Standard Model [5].

Since the current detection technologies rely on laser interferometry, the detectable frequency range is limited by the quantum nature of light (e.g. shot noise). To explore the frequency outside of the range 10 Hz - 10 kHz, a new detection method needs to be employed. The Terrestrial very-long-baseline atom interferometer (TVLBAI) is one such example [6]. This matter-wave interferometer is expected to be sensitive to GWs in deci-Hertz band, providing data in a frequency range unreachable by the current detection technology.

For high frequency GWs above 10 kHz, a detection possibility using cold atoms has been discussed [7]. Note that the effect of the gravity on the spectra of atoms and molecules has been previously investigated by several researchers [8–13], but previously believed to be impossible for a ground-based detection, due to the weakness of the signal. To improve the sensitivity, one may consider atoms in highly excited states, i.e. Rydberg states [14], or by looking at spectrum of atoms near GW sources e.g. interstellar medium.

In low-density regions of the interstellar medium (ISM), ions can capture free electrons at very high quan-

* nontapat@narit.or.th

† apimook@narit.or.th

tum numbers (typically $n > 100$) forming Rydberg atoms [15]. As these atoms undergo a cascade through lower high-lying states, each transition produces radio recombination lines (RRLs). These lines serve as valuable tracers of ionized environments, including HII regions and the diffuse ISM.

Advancements in radio astronomy, particularly with high-resolution instruments such as the Square Kilometre Array (SKA) and the Very Large Array (VLA), have significantly enhanced the ability to measure RRLs with greater precision [16, 17]. Observations have detected carbon RRLs from states with quantum numbers as high as $n = 1500$ in the cool, tenuous medium [18]. At such high excited states, these Rydberg atoms become extremely large, sometimes reaching macroscopic sizes, and are consequently fragile. The transitions between high-lying energy levels are highly sensitive to their surroundings, making them useful probes of local conditions such as temperature, density, and magnetic fields. A compelling question is whether these transitions also exhibit sensitivity to gravitational fields, e.g. near black holes or gravitational-wave sources. Investigating this possibility could provide insights into the observable effects of local gravity on atomic transitions in astrophysical environments.

This paper is organized as follows: In Sec. II, we derive the hyperfine structure modifications in the presence of GWs, using electrodynamics in curved spacetime. In Sec. III, we analyze the effects of GWs on hydrogen Rydberg states, including quantum mechanical and semi-classical approaches. Sec. IV focuses on GW-induced broadening in RRLs, comparing it to other broadening mechanisms and discussing its observational feasibility. In Sec. V, we consider the impact of the stochastic gravitational-wave background. Finally, in Sec. VI, we summarize our findings and propose potential avenues for future research.

II. EFFECTS OF GRAVITATIONAL WAVES ON THE HYPERFINE STRUCTURE

Consider a hydrogen atom in a gravitational field characterized by the Riemann curvature tensor $R^\alpha{}_{\beta\gamma\delta}$, where Greek indices denote spacetime coordinates. The primary contribution to the gravitational interaction Hamiltonian, H_I , arises from tidal interactions and is given by [7–9]:

$$H_I = \frac{1}{2} \mu c^2 R_{j0k0} x^j x^k, \quad (1)$$

where $\mu = m_e m_p / (m_e + m_p)$ is the reduced mass of the atom, c is the speed of light in vacuum, the coordinates x^0 and x^j indicate time and spatial coordinates in the atom's local inertial frame, respectively. For linearized gravitational waves, the curvature tensor takes the form:

$$R_{j0k0} = -\frac{1}{2c^2} \ddot{h}_{jk}^{\text{TT}}, \quad (2)$$

where h_{jk}^{TT} is the gravitational-wave tensor in the Transverse-Traceless (TT) gauge, and the double dots denote the second derivative with respect to time t .

Assuming the waves propagate in a well-defined direction $\hat{\mathbf{n}}$, we can write

$$h_{jk}^{\text{TT}}(t) = \sum_{A=+, \times} h_A(t) e_{jk}^A(\hat{\mathbf{n}}), \quad (3)$$

where $h_{+, \times}(t)$ are the waveforms for the plus and cross polarizations, and $e_{jk}^A(\hat{\mathbf{n}})$ is the polarization tensor defined by

$$e_{jk}^+(\hat{\mathbf{n}}) = \hat{\mathbf{u}}_j \hat{\mathbf{u}}_k - \hat{\mathbf{v}}_j \hat{\mathbf{v}}_k \quad (4a)$$

$$e_{jk}^\times(\hat{\mathbf{n}}) = \hat{\mathbf{u}}_j \hat{\mathbf{v}}_k + \hat{\mathbf{v}}_j \hat{\mathbf{u}}_k, \quad (4b)$$

where $\hat{\mathbf{u}}, \hat{\mathbf{v}}$ are unit vectors orthogonal to $\hat{\mathbf{n}}$ and to each other. We align the direction of gravitational-wave propagation along the z -axis, so that the components of h_{jk}^{TT} take the form

$$(h_{jk}^{\text{TT}}) = \begin{pmatrix} h_+(t) & h_\times(t) & 0 \\ h_\times(t) & -h_+(t) & 0 \\ 0 & 0 & 0 \end{pmatrix}. \quad (5)$$

From Eq. (2) and (1), the gravitational-wave tidal interaction Hamiltonian is

$$H_{\text{gw}} = \frac{1}{4} \mu \ddot{h}_{jk}^{\text{TT}} x^j x^k. \quad (6)$$

The objective in this section is to study the hyperfine structure in the presence of GWs. Specifically, we examine the effect of GWs on the interaction between atomic electron and nuclear magnetic dipole moments, which causes hyperfine splitting.

The hyperfine interaction Hamiltonian is given by

$$H_{\text{hf}} = -\vec{\mu}_S \cdot \vec{B}, \quad (7)$$

where $\vec{\mu}_S = -(e/m_e)\vec{S}$ is the electron's magnetic moment, and \vec{B} is the magnetic field generated by the proton's magnetic moment $\vec{\mu}_I = (g_p e/2m_p)\vec{I}$. Here, \vec{S} and \vec{I} are the electron and proton spins, respectively, and g_p is the proton's g-factor. In the absence of GWs, the magnetic field produced by the point-like magnetic dipole moment of the proton is given by

$$\vec{B} = \frac{\mu_0}{4\pi} \frac{3(\vec{I} \cdot \hat{x})\hat{x} - \vec{I}}{r^3} + \frac{2\mu_0}{3} \vec{I} \delta^3(\mathbf{x}), \quad (8)$$

where $\hat{x} \equiv \mathbf{x}/|\mathbf{x}|$ and $r \equiv |\mathbf{x}|$ is the distance between the proton and electron. This interaction leads to the well-known splitting of the ground state $1s^2S_{1/2}$ into two hyperfine levels.

When gravitational-wave effects are considered, the magnetic field expression in Eq. (8) must be modified to satisfy Maxwell's equations in curved spacetime. This

results in a correction to the magnetic field, which contributes to the hyperfine Hamiltonian. The corrected Hamiltonian can be expressed as

$$H_{\text{hf}} = H_{\text{hf}}^0 + \Delta H_{\text{hf}}^{\text{gw}}, \quad (9)$$

where H_{hf}^0 represents the unperturbed hyperfine interaction. Since the tidal interaction described by H_{gw} in Eq. (6) has no impact on the ground-state 1S energy level, as shown in Ref. [7], the only gravitational-wave contribution to the hyperfine structure is $\Delta H_{\text{hf}}^{\text{gw}}$.

A. Electrodynamics in gravitational-wave background

In quantum mechanics, electric and magnetic fields yield different effects on hydrogen spectra. To calculate such effects, one needs to make distinction between electric and magnetic fields in curved spacetime, which depends on the distinction between space and time in the chosen frame of reference. To do so, we employ the ADM formalism, which is decomposing the 4-dimensional spacetime into a stack of non-intersecting spatial hypersurfaces, Σ_t , labeled by a global time coordinate t . On each hypersurface, spatial coordinates x^j are introduced. The metric in this 3 + 1 decomposition takes the form

$$ds^2 = -\alpha^2(cdt)^2 + \gamma_{ij}(dx^i + \beta^i cdt)(dx^j + \beta^j cdt), \quad (10)$$

where α is the lapse function, β_i is the shift vector, and γ_{ij} is the induced metric on the spatial hypersurface Σ_t . From this, we can extract the components of the metric tensor, given by

$$(g_{\mu\nu}) = \begin{pmatrix} -\alpha^2 + \beta_k \beta^k & \beta_i \\ \beta_i & \gamma_{ij} \end{pmatrix}. \quad (11)$$

Here, $\beta_i = \gamma_{ij}\beta^j$, and $\beta^\mu = (0, \beta^i)$. Additionally, we have $\gamma^{00} = \gamma^{0i} = 0$.

The inverse metric, $g^{\mu\nu}$, is given by

$$(g^{\mu\nu}) = \begin{pmatrix} -\alpha^{-2} & \alpha^{-2}\beta^i \\ \alpha^{-2}\beta^i & \gamma^{ij} - \alpha^{-2}\beta^i\beta^j \end{pmatrix}, \quad (12)$$

where γ^{ij} is the inverse of γ_{ij} . It is important to note that $g_{ij} = \gamma_{ij}$, but $g^{ij} \neq \gamma^{ij}$ unless $\beta_j = 0$.

The determinant of the metric tensor, $g_{\mu\nu}$, is

$$g \equiv \det g_{\mu\nu} = -\alpha^2 \gamma, \quad (13)$$

where γ is the determinant of the induced metric γ_{ij} . This decomposition allows us to study the dynamics of spacetime in a convenient way, especially when considering perturbations such as gravitational waves.

For Eulerian observers, whose timelike worldlines are orthogonal to Σ_t , their 4-velocity components are expressed as

$$u_0 = -\alpha, \quad u_i = 0, \quad u^0 = \frac{1}{\alpha}, \quad u^i = -\frac{\beta^i}{\alpha}. \quad (14)$$

The induced metric in 4-tensor form can be written as

$$\gamma^{\mu\nu} = g^{\mu\nu} + u^\mu u^\nu, \quad (15)$$

which ensures that $\gamma^{\mu\nu}u_\mu = 0$, making γ^{ij} purely spatial.

In curved spacetime, the electromagnetic fields are described by the antisymmetric field tensor $F^{\mu\nu}$, which satisfies Maxwell's equations:

$$\nabla_\nu F^{\mu\nu} = \mu_0 J^\mu \quad (16a)$$

and

$$\epsilon^{\alpha\beta\gamma\delta} \nabla_\beta F_{\gamma\delta} = 0, \quad (16b)$$

where J^μ is charge-current 4-vector.

Maxwell's equations in the 3 + 1 formalism are derived in terms of physical quantities measured by observers with 4-velocity u^μ , such as the electric field E^j , magnetic field B^j , charge density ρ_e , and current density j^k . These fields are regarded as 4-vectors E^μ and B^μ on Σ_t , defined by

$$E^\mu = F^{\mu\nu}u_\nu, \quad E^\mu u_\mu = 0, \quad (17a)$$

$$B^\mu = -\frac{1}{2}\epsilon^{\mu\rho\sigma\nu}u_\rho F_{\sigma\nu}, \quad B^\mu u_\mu = 0. \quad (17b)$$

The Levi-Civita tensor $\epsilon^{\alpha\beta\gamma\delta}$ is given by

$$\epsilon_{\alpha\beta\gamma\delta} = \sqrt{-g}[\alpha\beta\gamma\delta], \quad \epsilon^{\alpha\beta\gamma\delta} = -\frac{1}{\sqrt{-g}}[\alpha\beta\gamma\delta] \quad (18)$$

where $[\alpha\beta\gamma\delta]$ denotes the permutation symbol. The charge and current densities are given by

$$\rho_e = -J^\mu u_\mu, \quad (19a)$$

$$j^\mu = \gamma^{\mu\nu}J_\nu. \quad (19b)$$

Conversely, the electromagnetic field tensor and charge-current density can be expressed in terms of the frame's 4-velocity as

$$F^{\mu\nu} = u^\mu(E^\nu/c) - u^\nu(E^\mu/c) + \epsilon^{\mu\nu\rho\sigma}u_\rho B_\sigma \quad (20a)$$

$$J^\mu = \rho_e u^\mu + j^\mu \quad (20b)$$

Substituting these into Maxwell's equations yields the 3 + 1 formalism of Maxwell's equations [19]:

$${}^{(3)}\nabla_k E^k = \frac{\rho_e}{\epsilon_0} \quad (21a)$$

$${}^{(3)}\nabla_k B^k = 0 \quad (21b)$$

$$D_u E^i + \frac{2}{3}\theta E^i - \gamma^{jk}\sigma^i_j E_k = -\frac{1}{\alpha}\epsilon^{ijk}{}^{(3)}\nabla_j(\alpha B_k) - 4\pi j^i \quad (21c)$$

$$D_u B^i + \frac{2}{3}\theta B^i - \gamma^{jk}\sigma^i_j B_k = -\frac{1}{\alpha}\epsilon^{ijk}{}^{(3)}\nabla_j(\alpha E_k). \quad (21d)$$

Here, ${}^{(3)}\nabla_k$ denotes the covariant derivative with respect to the induced metric γ_{ij} on Σ_t . The Fermi

time derivative of A^μ is defined as $D_u A^\alpha \equiv u^\mu \nabla_\mu A^\alpha - u^\alpha a_\mu A^\mu$, where $a_\mu = u^\nu \nabla_\nu u_\mu$ represents the frame's 4-acceleration. The Levi-Civita tensor on Σ_t is $\epsilon^{ijk} = \gamma^{-1/2}[ijk]$. The expressions for θ and $\sigma_{\mu\nu}$ are

$$\theta = \nabla_\mu u^\mu \quad (22)$$

$$\sigma_{\mu\nu} = \frac{1}{2} \gamma_\mu^\rho \gamma_\nu^\beta (\nabla_\beta u_\alpha + \nabla_\alpha u_\beta) - \frac{1}{3} \theta \gamma_{\mu\nu}. \quad (23)$$

In the weak-field gravity approximation, the spacetime metric is expressed as

$$g_{\mu\nu} = \eta_{\mu\nu} + h_{\mu\nu}, \quad |h_{\mu\nu}| \ll 1, \quad (24)$$

where $\eta_{\mu\nu} = \text{diag}(-1, 1, 1, 1)$ represents the flat Minkowski metric, and $h_{\mu\nu}$ is the perturbation. To first order in $h_{\mu\nu}$, the inverse metric is

$$g^{\mu\nu} = \eta^{\mu\nu} - h^{\mu\nu}. \quad (25)$$

The Christoffel connections are given by

$$\Gamma^\mu_{\rho\sigma} = \frac{1}{2} (h^\mu_{\rho,\sigma} + h^\mu_{\sigma,\rho} - h_{\rho\sigma}{}^{,\mu}) \quad (26)$$

To express the weak-field metric in ADM form, we use Eq. (11), (12), (24), and (25) to identify the lapse function and shift vector

$$\alpha = 1 - \frac{1}{2} h^{00}, \quad \beta_i = h_{i0}, \quad (27)$$

$$\beta^i = -h^{i0}, \quad \gamma_{ij} = \delta_{ij} + h_{ij}, \quad \gamma^{ij} = \delta^{ij} - h^{ij}. \quad (28)$$

The metric determinant is

$$g = -(1 + \eta^{\mu\nu} h_{\mu\nu}) = -(1 - h_{00} + \delta^{ij} h_{ij}) \quad (29)$$

For the normal observer, Eq. (14) gives

$$u^0 = 1 + \frac{1}{2} h^{00}, \quad u^i = h^{i0}, \quad u_0 = -\left(1 - \frac{1}{2} h^{00}\right), \quad u_i = 0 \quad (30)$$

These results hold for the linearized theory of GR in an arbitrary gauge.

To analyze the interaction between an atom and GWs, we adopt a proper reference frame co-moving along the atom's geodesic. In the vicinity of this geodesic, we introduce Fermi normal coordinates (FNC) $x^\mu = (ct, x^k)$, where t is the proper time parameterized the geodesic and x^k are Cartesian spatial coordinates. The spacetime metric in FNC can be expanded up to quadratic order of x^j , as follows [20]

$$g_{00} = -1 - R_{0l0m}(t) x^l x^m \quad (31a)$$

$$g_{0i} = -\frac{2}{3} R_{0lim}(t) x^l x^m \quad (31b)$$

$$g_{ij} = -\frac{1}{3} R_{iljm}(t) x^l x^m \quad (31c)$$

$$g^{00} = -1 + R_{0l0m}(t) x^l x^m \quad (31d)$$

$$g^{0i} = g_{0i} \quad (31e)$$

$$g^{ij} = \delta^{ij} + \frac{1}{3} R^i{}_{l}{}^j{}_{m}(t) x^l x^m, \quad (31f)$$

where the Riemann tensor is evaluated at spatial origin, i.e. along the atom geodesic, so it depends only on time t . For computational convenience, we choose the transverse-traceless (TT) gauge, so the Riemannian tensor takes the form (2). Consequently, we may redefine the above metric coefficients as

$$g_{00} = -1 + 2f, \quad g^{00} = -1 - 2f \quad (32a)$$

$$g_{0i} = g^{0i} = 0, \quad g_{ij} = g^{ij} = \delta_{ij} \quad (32b)$$

where we have defined

$$f \equiv \frac{1}{4c^2} \ddot{h}_{lm}^{\text{TT}}(t) x^l x^m \quad (33)$$

From Eq. (32), (27), (24), (25), one can deduces that the corresponding lapse, shift, and induced metric aom FNC of proper frame re

$$\alpha = 1 - f, \quad \beta_i = 0, \quad \gamma_{ij} = \delta_{ij}. \quad (34)$$

The frame's 4-velocity is thus

$$u^0 = 1 + f, \quad u_0 = -1 + f, \quad u_i = u^i = 0 \quad (35)$$

The Maxwell's equations (21) become

$$\partial_k E^k = \frac{\rho_e}{\epsilon_0} \quad (36a)$$

$$\partial_k B^k = 0 \quad (36b)$$

$$\frac{\partial B^j}{\partial t} + \epsilon_{jkl} \partial_k [(1-f)E_l] = 0 \quad (36c)$$

$$\epsilon_{jkl} \partial_k [(1-f)B_l] - \frac{\partial E^j}{\partial t} = \mu_0 j^j, \quad (36d)$$

which describe the electromagnetic fields in the presence of linearized GWs, consistent with the [21].

B. The hyperfine structure in the presence of gravitational waves

The magnetic field of a point-like magnetic dipole moment $\vec{\mu}$ that satisfies the Maxwell's equations in the presence of GWs, (36), is

$$\vec{B} = \frac{\mu_0}{4\pi} \frac{[3(\vec{\mu} \cdot \hat{x})\hat{x} - \vec{\mu}]}{r^3} \left(1 - \frac{1}{4c^2} \ddot{h}_{jk}^{\text{TT}} x^j x^k\right) + \frac{2\mu_0}{3} \vec{\mu} \delta^3(\mathbf{x}) \quad (37)$$

By comparing Eq. (37) with the corresponding expression in the absence of GWs, Eq. (8), one can deduce the correction to the standard hyperfine Hamiltonian as

$$\Delta H_{\text{hf}}^{(\text{gw})} = -K \ddot{h}_{lm}^{\text{TT}} \frac{x^l x^m}{r^3} [3(\vec{I} \cdot \hat{x})(\vec{S} \cdot \hat{x}) - \vec{I} \cdot \vec{S}], \quad (38)$$

where $K \equiv (g_p \mu_0 e^2) / (32\pi m_e m_p c^2)$.

We consider a sinusoidal gravitational wave with plus polarization and angular frequency ω_{gw} traveling along

the z -axis direction. In spherical coordinates, the relevant interaction term simplifies to

$$\ddot{h}_{jk}^{\text{TT}} x^j x^k = \omega_{\text{gw}}^2 h_+ r^2 \sin^2 \theta \cos 2\phi. \quad (39)$$

The matrix representation of the unperturbed hyperfine Hamiltonian H_{hf}^0 in the basis states $|n = 1, \ell = 0, m_\ell = 0; FM_F\rangle$ are diagonal, with the matrix elements

$$\langle 100; 00 | H_{\text{hf}}^0 | 100; 00 \rangle = -\frac{3}{4}A, \quad (40)$$

$$\langle 100; 1M'_F | H_{\text{hf}}^0 | 100; 1M_F \rangle = \frac{1}{4}A \delta_{M'_F M_F} \quad (41)$$

where

$$A = \frac{4g_p \hbar^4}{3m_p m_e^2 c^2 a^4}. \quad (42)$$

The presence of a gravitational wave introduces an additional perturbation, with matrix elements

$$\langle 100; F'M'_F | \Delta H_{\text{hf}}^{(\text{gw})} | 100; FM_F \rangle \quad (43)$$

$$= \frac{8\pi K}{5a} \omega_{\text{gw}}^2 h_+ \langle F'M'_F | \mathcal{S}_+ | FM_F \rangle. \quad (44)$$

where $\mathcal{S}_+ \equiv I_x S_x - I_y S_y$. To compute $\langle F'M'_F | \mathcal{S}_+ | FM_F \rangle$, we expand the coupled spin states $|FM_F\rangle$ in terms of the uncoupled basis $|s_1 m_1; s_2 m_2\rangle$. Here $s_1 = s_2 = 1/2$. Using the notation $|\frac{1}{2} \pm \frac{1}{2}; \frac{1}{2} \pm \frac{1}{2}\rangle \equiv |\pm \pm\rangle$, we express the states as

$$|00\rangle = \frac{1}{\sqrt{2}}(|+-\rangle - |-+\rangle) \quad (45a)$$

$$|11\rangle = |++\rangle \quad (45b)$$

$$|10\rangle = \frac{1}{\sqrt{2}}(|+-\rangle + |-+\rangle) \quad (45c)$$

$$|1-1\rangle = |--\rangle. \quad (45d)$$

A direct evaluation yields the only nonzero matrix elements:

$$\langle 1-1 | \mathcal{S}_+ | 11 \rangle = \langle 11 | \mathcal{S}_+ | 1-1 \rangle = \frac{\hbar^2}{2}. \quad (46)$$

From this, one obtains the matrix for H_{hf} in the coupled basis:

$$\begin{pmatrix} -\frac{3}{4}A & 0 & 0 & 0 \\ 0 & \frac{1}{4}A & 0 & B \\ 0 & 0 & \frac{1}{4}A & 0 \\ 0 & B & 0 & \frac{1}{4}A \end{pmatrix}, \quad B \equiv \frac{4\pi \hbar^2 K}{5a} \omega_{\text{gw}}^2 h_+. \quad (47)$$

By diagonalizing the matrix one obtains energies

$$E = -\frac{3}{4}A, \frac{A}{4}, \frac{A}{4} \pm B. \quad (48a)$$

The corresponding energy level diagram is shown in Fig. 1. The fractional frequency shift of the hyperfine splitting due to the gravitational wave perturbation is given by

$$\frac{\Delta\nu}{\nu} = \frac{2B}{A} \simeq 5.79 \times 10^{-30} \left(\frac{f_{\text{gw}}}{\text{MHz}} \right)^2 \left(\frac{h_+}{10^{-9}} \right), \quad (49)$$

indicating that the splitting induced by gravitational waves is extremely small and beyond the reach of current measurement technology.

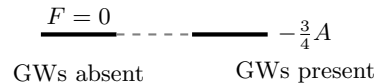
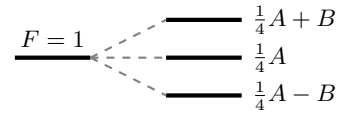


FIG. 1. Hyperfine structure of $1s^2S_{1/2}$ hydrogen in the absence and presence of gravitational waves.

III. EFFECT OF GRAVITATIONAL WAVES ON RYDBERG STATES

Another radiative process responsible for radio-frequency lines in hydrogen is the transition between states with high principal quantum numbers, i.e., Rydberg states. In this regime, the effects of GWs on both fine and hyperfine structure can be neglected, as the corresponding interactions weaken with increasing electron-nucleus separation, whereas the gravitational tidal interaction scales quadratically with distance. Thus, the relevant Hamiltonian is

$$H = H_0 + H_{\text{gw}}, \quad (50)$$

where

$$H_0 = \frac{p^2}{2\mu} - \frac{k}{r}, \quad k = \frac{e^2}{4\pi\epsilon_0}, \quad (51)$$

and H_{gw} is given in Eq. (6).

A. Quantum mechanical approach

In the quantum-mechanical framework of perturbation theory, the interaction Hamiltonian H_{gw} is introduced as a small perturbation to the Bohr Hamiltonian H_0 , consistent with the weak nature of gravitational waves. Given the significant degeneracy in hydrogen's energy levels, first-order degenerate perturbation theory is used to determine the associated energy shifts.

Expressed in spherical coordinates (r, θ, ϕ) , the perturbation Hamiltonian from Eq. (6) takes the form

$$H_{\text{gw}} = \frac{1}{4} \mu \omega_{\text{gw}}^2 r^2 \sin^2 \theta (h_+ \cos 2\phi + h_\times \sin 2\phi), \quad (52)$$

where the angular dependence can be expanded in terms of spherical harmonics $Y_\ell^m(\theta, \phi)$. Consider only the term containing h_+ , the first-order energy shifts are obtained by computing the eigenvalues of the perturbation matrix

$$\langle n\ell m | H_{\text{gw}}^+ | n\ell' m' \rangle = \kappa \mathcal{R}_{n\ell'}^{n\ell} \mathcal{F}_{\ell\ell'}^{m m'} \quad (53)$$

where, $\kappa \equiv \mu\omega_{\text{gw}}^2 h_+ / 4$. The radial and angular components are defined as

$$\mathcal{R}_{n\ell'}^{n\ell} \equiv \langle n\ell | r^2 | n\ell' \rangle \quad (54)$$

and

$$\mathcal{F}_{\ell\ell'}^{m m'} \equiv \sqrt{\frac{8\pi}{15}} \langle \ell m | (Y_2^2 + Y_2^{-2}) | \ell' m' \rangle. \quad (55)$$

For a given principal quantum number n , the perturbation matrix has dimensions $n^2 \times n^2$, therefore, numerically solving for eigenvalues requires increasingly high computation power for large n . Hence, deriving analytical expressions for the matrix elements in Eq. (53) becomes particularly useful at high n . The selection rules for the perturbation matrix elements $\langle n\ell m | H_{\text{gw}} | n\ell' m' \rangle$, as established in Ref. [7], dictate that nonzero values occur only when

$$\Delta\ell \equiv \ell' - \ell = 0, \pm 2 \quad (56a)$$

and

$$\Delta m \equiv m' - m = \pm 2. \quad (56b)$$

For the nonzero elements, we derive explicit analytical formulas for the relevant radial and angular components using the methods detailed in Appendix A and B. However, since obtaining an exact analytical form of the eigenvalues, is not practical with this approach, we introduce a semi-classical treatment in the next subsection.

B. Semi-classical approach

In the classical hydrogen atom model, the electron's motion within the Coulomb potential follows a Keplerian orbit, with a total energy $E < 0$. The corresponding Hamiltonian, H_0 , is given by Eq. (51). Both the total energy E and the orbital angular momentum L are conserved, reflecting the static and isotropic nature of the Coulomb potential.

When a gravitational wave is present, the interaction between the atom and the wave, within the Newtonian framework, is described by $H_{\text{gw}} = \mu\Phi_{\text{gw}}$, where the gravitational potential $\Phi_{\text{gw}} = -(1/4)\omega_{\text{gw}}^2 h_{jk}^{\text{TT}} x^j x^k$. To calculate this energy shift, we use classical perturbation theory i.e. averaging the perturbation Hamiltonian over the unperturbed motion of the electron. Specifically, for this system, the perturbation Hamiltonian H_{gw} is averaged over one orbital period τ_0 of the electron's Keplerian motion, denoted as $\langle \dots \rangle_0$,

$$\delta E_{\text{gw}} = \langle H_{\text{gw}} \rangle_0 \equiv \frac{1}{\tau_0} \int_0^{\tau_0} H_{\text{gw}} dt. \quad (57)$$

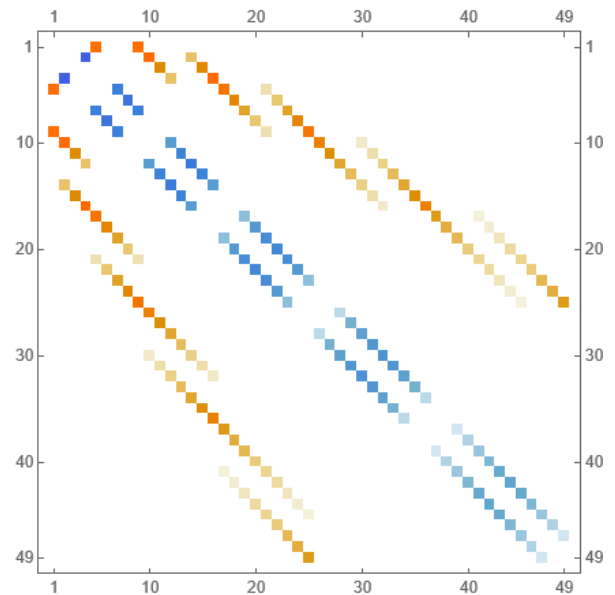


FIG. 2. Matrix representation of gravitational-wave perturbation in the energy level $n = 7$ of hydrogen, which exhibits 49-fold degeneracy. The structure is sparse and banded, with distinct groupings of nonzero elements, reflecting selection rules imposed by gravitational-wave coupling.

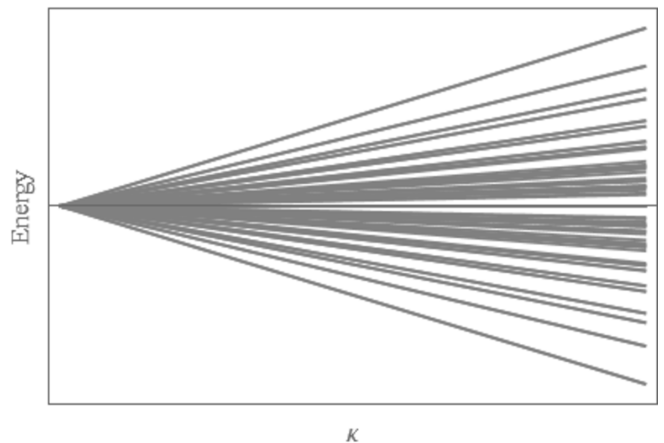


FIG. 3. Splitting of the $n = 9$ hydrogen energy level due to gravitational-wave perturbation. GWs lift the degeneracy, distributing the energy levels according to selection rules. Each line represents a sublevel's shift under the perturbation, with κ indicating the perturbation strength.

To simplify the computation of the term $h_{jk}^{\text{TT}} x^j x^k$, we choose to work in a rotated coordinate frame (x', y', z') , where the electron's orbit lies entirely in the $x'y'$ -plane. As shown in Fig. 4, this new frame is related to the original frame by two successive rotations: one by an angle ι around the y -axis, followed by another by an angle φ around the z -axis. This transformation is represented

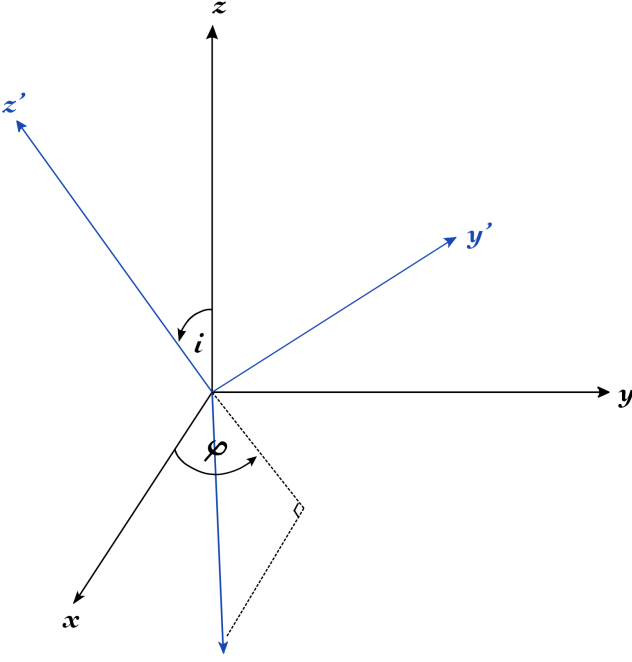


FIG. 4. The transformation from the original coordinate system (x, y, z) to the rotated frame (x', y', z') , where the electron's orbit lies in the $x'y'$ -plane.

by the rotation matrix \mathcal{R}_{ij} :

$$(\mathcal{R}_{ij}) = \begin{pmatrix} \cos \varphi & \sin \varphi & 0 \\ -\sin \varphi & \cos \varphi & 0 \\ 0 & 0 & 1 \end{pmatrix} \begin{pmatrix} \cos \iota & 0 & \sin \iota \\ 0 & 1 & 0 \\ -\sin \iota & 0 & \cos \iota \end{pmatrix}. \quad (58)$$

Each component $h_{i'j'}^{\text{TT}}$ in the rotated frame (x', y', z') is given by

$$h_{i'j'}^{\text{TT}} = \mathcal{R}_{ik} \mathcal{R}_{jl} h_{kl}^{\text{TT}}. \quad (59)$$

For ease in the mathematical expressions, and without significantly affecting the physical estimation of the energy shift, we set $\varphi = 0$ for the following calculations. In the rotated coordinate frame, the components of the gravitational wave field are

$$h_{x'x'} = h_+ \cos^2 \iota, \quad h_{y'y'} = -h_+, \quad h_{x'y'} = h_{y'x'} = h_\times \cos \iota. \quad (60)$$

The electron's position in this frame can be described using polar coordinates (r, ψ) as

$$x' = r \cos \psi, \quad y' = r \sin \psi, \quad z' = 0, \quad (61)$$

where the radial coordinate r is given by

$$r = \frac{L^2}{\mu k} [1 + \epsilon \cos \psi]^{-1}, \quad (62)$$

with L representing the classical orbital angular momentum and ϵ the orbital eccentricity. Substituting these

into Eq. (6) results in

$$H_{\text{gw}} = \frac{\mu \omega_{\text{gw}}^2 r^2}{4} \{ h_+ [(\cos^2 \iota + 1) \cos \psi - 1] + h_\times \cos \iota \sin 2\psi \} \quad (63)$$

To evaluate the energy shift, we change variables from t to ψ in the integral from Eq. (57), using the relation

$$dt = \frac{\mu r^2}{L} d\psi. \quad (64)$$

This gives

$$\delta E_{\text{gw}} = \frac{\mu}{L \tau_0} \int_0^{2\pi} r^2 H_{\text{gw}} d\psi. \quad (65)$$

Under the assumption that the gravitational wave frequency is significantly lower than the electron's orbital frequency (the adiabatic regime), the time-dependent variation of the GW amplitude can be considered negligible. Consequently, it remains effectively constant over one orbital period. This condition is satisfied when

$$\omega_{\text{gw}} \ll \frac{\alpha c}{a_0 n^3}, \quad (66)$$

where α is the fine-structure constant.

By substituting (62) and (64) into (65) and completing the integration, we get

$$\delta E_{\text{gw}} = \frac{\pi \omega_{\text{gw}}^2 L^7 h_+}{8k^4 \mu^2 \tau_0} \times \left[\frac{(2 \cos^2 \iota - 1) \epsilon (\epsilon^2 + 4) + 3\epsilon^3 + 6\epsilon^2 + 12\epsilon + 4}{(1 - \epsilon^2)^{7/2}} \right]. \quad (67)$$

Note that only the plus polarization component contributes to the energy shift.

The action variables are introduced as follows [22]:

$$I_1 = L_z, \quad (68a)$$

$$I_2 = L, \quad (68b)$$

$$I_3 = \sqrt{-\frac{\mu k^2}{2H_0}}. \quad (68c)$$

These are associated with the angle variables $\phi_1, \phi_2,$ and ϕ_3 , representing the longitude of the ascending node, the argument of perihelion, and the mean anomaly, respectively. The action variables are constrained by $|I_1| \leq I_2 \leq I_3$. The orbital inclination ι , eccentricity ϵ , and the period of the Kepler orbit τ_0 can be expressed in terms of the action variables as

$$\cos \iota = \frac{I_1}{I_2}, \quad \epsilon = \sqrt{1 - \left(\frac{I_2}{I_3}\right)^2}, \quad \tau_0 = \frac{2\pi I_3^2}{\mu k^2} \quad (69)$$

According to the Wilson-Sommerfeld quantization rule, each classical action variable I_k is quantized as follows:

$$I_k = \oint p_k dq_k = n_k \hbar \quad (70)$$

This leads to the specific quantization conditions

$$I_1 = m\hbar, \quad I_2 = \ell\hbar, \quad I_3 = n\hbar, \quad (71)$$

where m , ℓ , and n are integers representing quantum numbers associated with each action variable. Notably, quantizing I_3 in Eq. (68c) yields the Bohr energy levels

$$\delta E_{n\ell m}^{\text{gw}} = \frac{5\mu a^2 \omega_{\text{gw}}^2 h_+}{8} n^4 \left[1 - \frac{3}{5} \left(\frac{\ell}{n} \right)^2 + \left\{ 1 - \frac{1}{5} \left(\frac{\ell}{n} \right)^2 + \left(\frac{m}{\ell} \right)^2 - \frac{1}{5} \left(\frac{m}{n} \right)^2 \right\} \sqrt{1 - \left(\frac{\ell}{n} \right)^2} \right]. \quad (73)$$

Here, $a = (m_e/\mu)a_0$ and a_0 is the Bohr radius. However, this result in Eq. (73) becomes problematic as $n \rightarrow \infty$ because it diverges, while in reality, the atom would ionize before reaching such high states. Moreover, recall that this result was derived under the perturbative assumption that $H_{\text{gw}} \ll H_0$. Therefore, the approximation remains valid as long as $\delta E_{n\ell m}^{\text{gw}} \ll E_n^{\text{Bohr}}$ and the adiabatic condition in Eq. (66) holds.

IV. BROADENING IN HYDROGEN RRLS

The radiative transition from $n+1$ to n in the hydrogen atom, referred to as $Hn\alpha$, occurs within the radio-frequency range for $n \gtrsim 100$. The corresponding frequency is approximately given by

$$\nu_0 \simeq \frac{k}{an^3} \approx \frac{6.576 \times 10^{15} \text{ Hz}}{n^3}, \quad (74)$$

where $a = a_0(m_e/\mu)$ and a_0 is the Bohr radius.

As discussed previously, the presence of GWs induces energy shifts in the atomic states, breaking the degeneracy of the Bohr energy level n . This results in sub-levels symmetrically distributed around the original unperturbed level. As a result, the spectral lines for transitions such as $Hn\alpha$ exhibit broadening, providing a potential signature of GW interactions with atoms. The linewidth broadening of the $Hn\alpha$ transition caused by GWs is quantified by $\Delta\nu = (\delta E_{(n+1)\ell'm'}^{\text{gw}} + \delta E_{n\ell m}^{\text{gw}})/h$, where h is Planck's constant.

Specifically, for high n , the semi-classical formula, Eq. (73), and (74) gives

$$\begin{aligned} \left(\frac{\Delta\nu}{\nu_0} \right)_{\text{gw}} &= \frac{\mu a^3 \omega_{\text{gw}}^2 h_+ n^7}{2k} \\ &\simeq 2.53 \times 10^{-7} \left(\frac{f_{\text{gw}}}{1 \text{ GHz}} \right)^2 \left(\frac{h_c}{10^{-10}} \right) \left(\frac{n}{300} \right)^7. \end{aligned} \quad (75)$$

The spectral resolving power R required to measure the GW-induced linewidth of the $Hn\alpha$ transition for large

for the hydrogen atom:

$$H_0 = - \left(\frac{\mu k^2}{2\hbar^2} \right) \frac{1}{n^2} = E_n^{\text{Bohr}}. \quad (72)$$

By substituting Eq. (71) and (68) into (67), we obtain

values of n is given by

$$R \simeq \left(\frac{\Delta\nu}{\nu_0} \right)_{\text{gw}}^{-1} \quad (76)$$

$$\simeq 5.93 \times 10^8 \left(\frac{300}{n} \right)^6 \left(\frac{1 \text{ GHz}}{f_{\text{gw}}} \right)^2 \left(\frac{10^{-10}}{h_+} \right), \quad (77)$$

and for a given resolving power R , the detectable gravitational-wave amplitude is

$$h_{\text{det}} = \text{O} \left(\frac{\mu a^3 \omega_{\text{gw}}^2 n^7}{2kR} \right). \quad (78)$$

We can use this quantity to represent the detection sensitivity.

When comparing different broadening mechanisms, the most fundamental contributions are natural broadening.

$$\left(\frac{\Delta\nu}{\nu_0} \right)_{\text{rad}} = \frac{1}{2\pi\nu_0} \Gamma_0, \quad (79)$$

where Γ_0 is the sum of the total rate of spontaneous decay for Rydberg states of principal quantum numbers $n+1$ and n , which are approximately equal and given by the sum of Einstein-A coefficients $A_{nn'}$ for $n' < n$:

$$\Gamma_0 = \Gamma_{n+1} + \Gamma_n \simeq 2\Gamma_n = 2 \sum_{n' < n} A_{nn'}. \quad (80)$$

In addition, interstellar atoms exist in a finite-temperature environment permeated by blackbody radiation (BBR), such as the cosmic microwave background (CMB). As a result, BBR-induced broadening must be accounted for in the study of Rydberg states [23, 24]:

$$\left(\frac{\Delta\nu}{\nu_0} \right)_{\text{BBR}} = \frac{1}{2\pi\nu_0} \Gamma_{\text{BBR}}, \quad (81)$$

where Γ_{BBR} is the total rate of BBR-induced transitions:

$$\Gamma_{\text{BBR}} = \sum_{n'} \frac{A_{nn'}}{\exp(\hbar\omega_{nn'}/k_B T) - 1}. \quad (82)$$

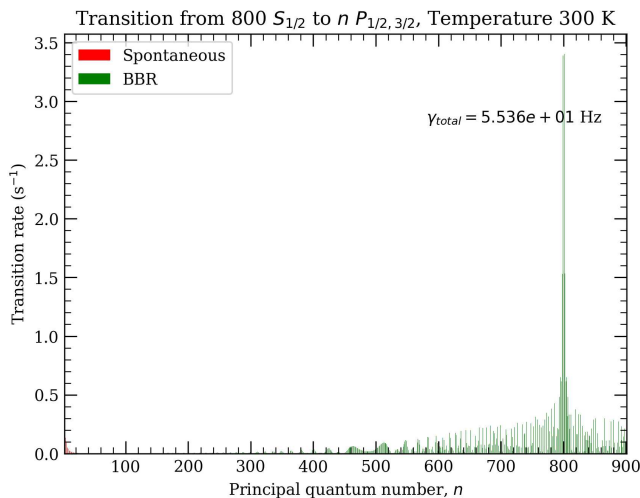


FIG. 5. Transition rates due to BBR at $T = 300$ K and spontaneous decay for hydrogen at $n = 800$.

For analytical convenience, an approximate expression valid for $n > 20$ (see section 5.4.1 of Ref. [25]) can be used:

$$A_{nn'} = \frac{2A_0}{n^3 n' (n^2 - n'^2)}, \quad (83)$$

$$\sum_{n' < n} A_{nn'} = \frac{A_0}{n^5} \ln \left(\frac{n^3 - n}{2} \right) \quad (84)$$

where $A_0 = 7.89 \times 10^9 \text{s}^{-1}$.

In addition, interstellar atoms exist in various astrophysical environments with different local temperatures and pressures, which influence their atomic spectra and must be taken into account. One of the dominant broadening mechanisms in the observation of RRLs is Doppler broadening. The Doppler linewidth due to the thermal motion of hydrogen gas with kinetic temperature T (in Kelvin) is given by [26]

$$\left(\frac{\Delta\nu}{\nu_0} \right)_{\text{Doppler}} = \left(\frac{(8 \ln 2) k_B T}{m_H c^2} \right)^{1/2} \simeq (7.137 \times 10^{-7} \text{K}^{-1/2}) \sqrt{T}. \quad (85)$$

However, direct calculations using the Alkali Rydberg Calculator (ARC) [27] indicate that for the lowest possible BBR temperature corresponding to the CMB, i.e. $T = 3$ K, BBR-induced transitions are negligible. Figure 5 illustrates the transition rates due to BBR at $T = 300$ K compared to spontaneous decay for hydrogen at $n = 800$.

As a constraint on Doppler broadening, the lowest natural temperature in the universe, in the absence of other heating mechanisms, is set by the cosmic microwave background (CMB) at approximately 2.73 K. Interstellar hydrogen gas can cool to near this temperature through radiative equilibrium with the CMB. In such cases, the Doppler broadening is 1.78×10^{-6} .

In addition to the aforementioned broadening, another significant effect contributing to spectral line broadening arises from the immersion of hydrogen atoms in a high-density neutral background. Interactions between hydrogen atoms in the Rydberg state and the background gas result in two dominant effects: energy level shifts and spectral line broadening [28, 29]. For a Rydberg state with principal quantum number n , the resulting line broadening can be expressed as

$$\left(\frac{\Delta\nu}{\nu_0} \right)_{\text{sc}} = \frac{a_s N \hbar}{m_e k} a n^3, \quad (86)$$

where a_s is the s-wave scattering length of background gas and N is the volume density of the background gas.

Additionally, when hydrogen atoms are in the Rydberg state, the large separation between the electron and proton allows the background gas to occupy the Rydberg-atom volume. The background gas is then subject to the electric field generated by the Rydberg hydrogen atoms. This phenomenon, known as polarization-induced decay, contributes to the additional linewidth in the hydrogen Rydberg spectra,

$$\left(\frac{\Delta\nu}{\nu_0} \right)_{\text{p}} = \frac{6.21}{2\pi k} \left[\frac{\alpha e^2 \hbar^2}{k} \right]^{2/3} a n^3 v^{1/3} N, \quad (87)$$

where α is the polarizability of the background gas and v is the mean relative velocity between the hydrogen atoms and the background gas. In general, $(\Delta\nu/\nu_0)_{\text{p}}$ is larger than $(\Delta\nu/\nu_0)_{\text{sc}}$ and the total linewidth according to these two affect becomes $(\Delta\nu/\nu_0)_{\text{sc}} + (\Delta\nu/\nu_0)_{\text{p}}$.

Note that although we have primarily considered hydrogen so far, this analysis also applies to the RRLs of other species. Any atom in a Rydberg state can be treated approximately as a hydrogen-like system with a different reduced mass.

The characteristic amplitude of quadrupolar gravitational-wave emission from a compact binary system consisting of point-like masses m_1 and m_2 in quasi-circular Newtonian orbits is given by

$$h_c = \frac{4}{D} \left(\frac{G\mathcal{M}}{c^2} \right)^{5/3} \left(\frac{\pi f_{\text{gw}}}{c} \right)^{2/3} \quad (88)$$

where $\mathcal{M} = (m_1 m_2)^{3/5} / (m_1 + m_2)^{1/5}$ is the binary chirp mass, and D represents the distance between the source and observer.

For binary systems made up of compact objects like black holes or neutron stars, the inspiral phase ends when the objects reach the innermost stable circular orbit (ISCO), as determined by Schwarzschild geometry. This occurs when the separation between the objects reduces to $r_{\text{ISCO}} = 6G(m_1 + m_2)/c^2$. After this point, the objects spiral inward, and the strong-field dynamics begin to influence the system's evolution. At this stage, the GW waveform can no longer be described by the linearized theory of general relativity that is assumed here. For compact binary inspirals, the frequency of the GW

at ISCO, which marks the peak frequency of the inspiral phase, is given by

$$f_{\text{gw}}^{\text{ISCO}} = \frac{1}{6\sqrt{6}\pi} \frac{c^3}{GM} \simeq 4400 \text{ Hz} \left(\frac{M_{\odot}}{M} \right) \quad (89)$$

where $M = m_1 + m_2$. The corresponding characteristic amplitude is

$$h_c^{\text{ISCO}} \simeq \frac{2}{3} \frac{G}{c^2} \frac{\mu_s}{D} \simeq 6.56 \times 10^{-6} \left(\frac{\mu_s}{M_{\odot}} \right) \left(\frac{1 \text{ AU}}{D} \right) \quad (90)$$

where $\mu_s = m_1 m_2 / (m_1 + m_2)$.

Binary inspirals of stellar-mass or massive black holes with masses greater than $3M_{\odot}$ produce GW frequencies at ISCO below 100 Hz. To generate GWs with peak frequencies above 10 kHz and up to the GHz range, the

component masses in the binary system must be on the order of $\sim 10^{-1} - 10^{-6} M_{\odot}$. Such masses are too small for the objects to be stellar-mass black holes or even the smallest neutron stars. Instead, these sub-solar-mass compact objects could be primordial black holes (PBHs) with planetary masses. PBHs are theorized to form in the early Universe through various mechanisms and are considered potential candidates for dark matter (see [30–32] for reviews). Unlike stellar-mass black holes, PBHs can have a wide range of masses, from as small as the Planck mass (10^{-5} g) to as large as $10^5 M_{\odot}$. The GW-induced broadening of RRLs presents a promising observational method for detecting such signals and could provide a new way to confirm the existence of small PBHs formed in the early Universe.

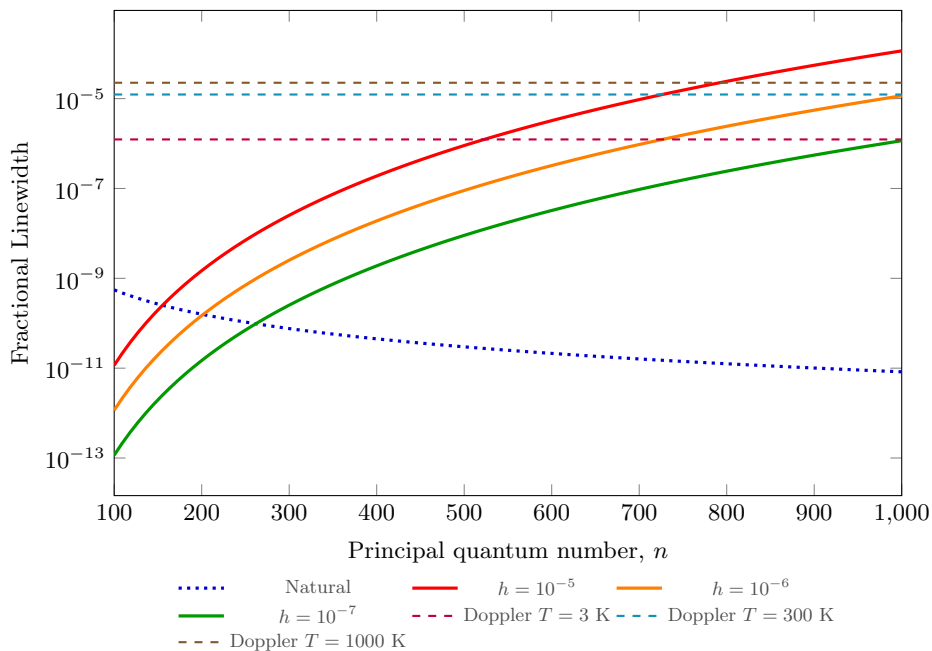


FIG. 6. Fractional linewidth contributions from natural broadening, gravitational-wave broadening induced by a MHz-frequency GW from a $10^{-3} M_{\odot}$ PBH in a binary inspiral at various distances, and Doppler broadening, for hydrogen atoms with principal quantum number n .

V. STOCHASTIC GRAVITATIONAL-WAVE BACKGROUND

Previously, we analyzed gravitational waves as nearly monochromatic signals with a well-defined angular frequency ω_{gw} , traveling in a single direction through atomic systems, typically originating from isolated periodic sources. However, a more general case to consider is

the stochastic gravitational-wave background (SGWB), which consists of a random superposition of waves arriving from all directions, covering a broad spectrum of frequencies and amplitudes. At the atom's location $\mathbf{x} = 0$, the SGWB is described by

$$h_{jk}^{\text{TT}}(t) = \sum_{A=+, \times} \int d^2 \hat{\mathbf{n}} e_{jk}^A(\hat{\mathbf{n}}) \int df \tilde{h}_A(f, \hat{\mathbf{n}}) e^{-2\pi f t i}. \quad (91)$$

Here $\hat{\mathbf{n}}$ denotes the wave propagation direction, with $d^2\hat{\mathbf{n}} = d\cos\theta d\phi$. The Fourier amplitude $\tilde{h}_A(f, \hat{\mathbf{n}})$ satisfies the statistical condition

$$\langle \tilde{h}_A^*(f, \hat{\mathbf{n}}) \tilde{h}_A(f', \hat{\mathbf{n}}') \rangle = \delta_{AA'} \delta(f - f') \frac{\delta^2(\hat{\mathbf{n}}, \hat{\mathbf{n}}')}{4\pi} \frac{1}{2} S_h(f), \quad (92)$$

where $\langle \dots \rangle$ denotes the ensemble average, and $\delta^2(\hat{\mathbf{n}}, \hat{\mathbf{n}}') = \delta(\phi - \phi') \delta(\cos\theta - \cos\theta')$. The function $S_h(f)$ is the single-sided spectral density of the SGWB, which is related to the energy density per unit logarithmic frequency

$$\Omega_{\text{gw}}(f) = \frac{1}{\rho_c} \frac{d\rho_{\text{gw}}}{d\log f}, \quad (93)$$

where ρ_c is the critical density, by the relationship

$$S_h(f) = \frac{3H_0^2}{4\pi^2 f^3} \Omega_{\text{gw}}(f). \quad (94)$$

The classical Hamiltonian described the tidal interaction between the SGWB and a hydrogen atom is

$$H_I = \frac{1}{4} \mu r^2 \times \sum_{A=+, \times} \int d^2\hat{\mathbf{n}} \hat{x}^j \hat{x}^k e_{jk}^A(\hat{\mathbf{n}}) \int df (2\pi f)^2 \tilde{h}_A(f, \hat{\mathbf{n}}) e^{-2\pi f t i}, \quad (95)$$

where $r^2 \equiv \delta_{jk} x^j x^k$ and $\hat{x}^i = x^i/r$. From this one can view the atom as a tensor operator, denoted by D^{jk} , that maps the GW tensor $\tilde{h}_{jk}^{\text{TT}}$ onto a scalar quantity representing the interaction Hamiltonian: $H_I = D^{jk} h_{jk}^{\text{TT}}$. Here $D^{jk} = (1/4) \mu x^j x^k$. The corresponding *detector pattern function* is given by

$$F^A(\hat{\mathbf{n}}) = \hat{x}^j \hat{x}^k e_{jk}^A(\hat{\mathbf{n}}), \quad (96)$$

which depends on the wave's propagation direction (θ, ϕ) .

The effective interaction Hamiltonian is

$$H_I^{\text{eff}} = \sqrt{\langle H_I^2(t) \rangle} = \frac{1}{4} \mu r^2 F \left[\int_0^\infty df (2\pi f)^2 S_h(f) \right]^{1/2} \quad (97)$$

where

$$F^2 \equiv \sum_{A=+, \times} \int_0^{2\pi} \frac{d\psi}{2\pi} \int \frac{d^2\mathbf{n}}{4\pi} F^A(\hat{\mathbf{n}}, \psi) F^A(\hat{\mathbf{n}}, \psi). \quad (98)$$

By straightforward calculation, described in Appendix C, we find that $F^2 = 8\pi/15$.

Using this result, the energy shifts induced by the SGWB can be computed via perturbation theory, as discussed previously.

VI. CONCLUSION AND OUTLOOK

This paper examines how GWs affect hydrogen radio-frequency spectral lines, particularly through hyperfine

splitting and broadening in RRLs. Using both quantum-mechanical and semi-classical methods, we show that GWs cause potentially detectable energy shifts in highly excited states of hydrogen atoms, resulting in spectral broadening that the fractional linewidth scales with $n^7 \omega_{\text{gw}}^2 h(t)$. This suggests that high- n RRLs could serve as astrophysical probes for ultra-high-frequency GWs.

Our theoretical analysis indicates that GW-induced broadening could dominate over natural broadening in specific astrophysical environments, particularly for inspiraling primordial black hole binaries with planetary masses. While present-day radio telescopes may lack the resolution to observe this effect, next-generation spectroscopic facilities like the SKA should be able to achieve such detectability. Additionally, studying the impact of a stochastic gravitational-wave background on hydrogen spectral lines offers a potential avenue for indirect GW detection.

This work establishes atomic spectroscopy as a promising tool for gravitational-wave astronomy. Future studies could refine these predictions by incorporating interstellar environmental factors, enhancing observational techniques, and investigating potential GW signatures from astrophysical sources.

ACKNOWLEDGMENTS

This research has received funding support from the NSRF via the Program Management Unit for Human Resources & Institutional Development, Research and Innovation [grant number B39G680007]. We also thank Prof. Hoi Lai, Yu for his valuable comments and suggestion.

Appendix A: The angular matrix elements ($\mathcal{F}_{\ell\ell'}^{mm'}$)

The angular matrix element $\mathcal{F}_{\ell\ell'}^{mm'}$ defined in Eq. (55). These matrix elements can be evaluated using the integral

$$\begin{aligned} \langle \ell m | Y_2^{\pm 2} | \ell' m' \rangle &= \int Y_\ell^{*m}(\theta, \phi) Y_2^{\pm 2}(\theta, \phi) Y_{\ell'}^{m'}(\theta, \phi) d\Omega \\ &= (-1)^{-m} \sqrt{\frac{5}{4\pi}} (2\ell + 1)(2\ell' + 1) \begin{pmatrix} \ell & 2 & \ell' \\ 0 & 0 & 0 \end{pmatrix} \begin{pmatrix} \ell & 2 & \ell' \\ m & \pm 2 & m' \end{pmatrix} \end{aligned} \quad (\text{A1})$$

where the 2×3 matrices are the Wigner $3j$ -symbols. The non-zero elements of $\mathcal{F}_{\ell\ell'}^{m,m'}$ are given by

$$\mathcal{F}_{\ell\ell}^{m,m+2} = -\frac{1}{(2\ell-1)(2\ell+3)} \sqrt{\frac{(\ell-m)!(\ell+m+2)!}{(\ell+m)!(\ell-m-2)!}} \quad (\text{A2})$$

$$\mathcal{F}_{\ell\ell}^{m,m-2} = -\frac{1}{(2\ell-1)(2\ell+3)} \sqrt{\frac{(\ell+m)!(\ell-m+2)!}{(\ell-m)!(\ell+m-2)!}} \quad (\text{A3})$$

$$\mathcal{F}_{\ell,\ell+2}^{m,m+2} = \frac{1}{2(2\ell+1)} \sqrt{\frac{(\ell+m+4)!}{(\ell+m)!(2\ell+1)(2\ell+5)}} \quad (\text{A4})$$

$$\mathcal{F}_{\ell,\ell+2}^{m,m-2} = \frac{1}{2(2\ell+3)} \sqrt{\frac{(\ell-m+4)!}{(\ell-m)!(2\ell+1)(2\ell+5)}} \quad (\text{A5})$$

$$\mathcal{F}_{\ell,\ell-2}^{m,m+2} = \frac{1}{2(2\ell+1)} \sqrt{\frac{(\ell+m+4)!}{(\ell+m)!(2\ell+1)(2\ell+5)}} \quad (\text{A6})$$

$$\mathcal{F}_{\ell,\ell+2}^{m,m-2} = \frac{1}{2(2\ell+3)} \sqrt{\frac{(\ell-m)!}{(\ell-m-4)!(2\ell-3)(2\ell+1)}} \quad (\text{A7})$$

$$(\text{A8})$$

Appendix B: Evaluation of radial matrix elements of the form $\langle n\ell|r^2|n\ell' \rangle$

To calculate the radial quadrupolar matrix element for the hydrogen atom, we consider the expression

$$\langle n\ell|r^2|n\ell' \rangle = \int_0^\infty r^4 R_{n\ell}(r) R_{n\ell'}(r) dr \quad (\text{B1})$$

where $R_{n\ell}$ represents the radial wavefunction of hydrogen,

$$R_{n\ell}(r) = N_{n\ell} x^\ell e^{-x/2} L_{n-\ell-1}^{2\ell+1}(x) \quad (\text{B2})$$

with $x \equiv 2r/na$ and $N_{n\ell}$ being the normalization constant:

$$N_{n\ell} = \sqrt{\left(\frac{2}{na}\right)^3 \frac{(n-\ell-1)!}{2n(n+\ell)!}}. \quad (\text{B3})$$

Evaluating the matrix element in Eq. (B1) involves computing an integral of the form

$$\int_0^\infty e^{-x} x^{\ell+\ell'} x^4 L_{n-\ell-1}^{2\ell+1}(x) L_{n-\ell'-1}^{2\ell'+1}(x) dx. \quad (\text{B4})$$

For this purpose, the following recursion relation for the associated Laguerre polynomials is useful (reference: [33]):

$$xL_q^p = (p+2q+1)L_q^p - (q+1)L_{q+1}^p - (p+q)L_{q-1}^p \quad (\text{B5})$$

along with the orthogonality relation

$$\int_0^\infty e^{-x} x^k L_m^k(x) L_n^k(x) dx = \frac{(k+m)!}{m!} \delta_{mn}. \quad (\text{B6})$$

Using these relations, one can systematically simplify and evaluate the integral in Eq. (B4), ultimately leading to an explicit expression for the desired radial matrix element (B1).

The radial matrix elements used to construct the perturbation matrix (52) are

$$\langle n\ell|r^2|n\ell \rangle = \frac{5a^2n^2}{2} \left[n^2 + \frac{1-3\ell(\ell+1)}{5} \right] \quad (\text{B7})$$

$$\langle n\ell|r^2|n,\ell+2 \rangle = \frac{5a^2n^2}{2} \sqrt{\frac{(n-\ell-1)!(n+\ell+2)!}{(n+\ell)!(n-\ell-3)!}} \quad (\text{B8})$$

$$\langle n\ell|r^2|n,\ell-2 \rangle = \frac{5a^2n^2}{2} \sqrt{\frac{(n+\ell)!(n-\ell+1)!}{(n-\ell-1)!(n+\ell-2)!}} \quad (\text{B9})$$

Appendix C: Computing the angular efficiency factor

We provide a brief guide to computing the detector pattern function $F^A(\hat{\mathbf{n}})$ and the angular efficiency factor F^2 for the hydrogen atom as a probe of SGWB described

by Eq. (91). In spherical polar coordinates, we can write

$$\hat{\mathbf{n}} = \begin{pmatrix} \sin \theta \sin \phi \\ \sin \theta \cos \phi \\ \cos \theta \end{pmatrix}, \quad \hat{x} = \begin{pmatrix} \sin \theta' \sin \phi' \\ \sin \theta' \cos \phi' \\ \cos \theta' \end{pmatrix}, \quad (\text{C1})$$

$$\mathbf{u} = \begin{pmatrix} -\cos \theta \sin \phi \cos \psi - \cos \phi \sin \psi \\ -\cos \theta \cos \phi \cos \psi + \sin \phi \sin \psi \\ \sin \theta \cos \phi \end{pmatrix}, \quad (\text{C2})$$

$$\hat{\mathbf{v}} = \begin{pmatrix} \cos \theta \sin \phi \sin \psi - \cos \phi \cos \psi \\ \cos \theta \cos \phi \sin \psi + \sin \theta \cos \psi \\ -\sin \theta \sin \psi \end{pmatrix}. \quad (\text{C3})$$

Using Eq. (96) together with the expression for the polarization tensor e_{jk}^A , given in Eq. (4), we obtain the pattern functions

$$F^+(\theta, \phi, \psi) = \sin 2\psi [\sin 2\theta' \sin \theta \sin(\phi' - \phi) - \sin^2 \theta' \cos \theta \sin 2(\phi' - \phi)] - \frac{1}{4} \cos 2\psi [\sin^2 \theta' (\cos 2\theta + 3) \cos 2(\phi' - \phi) - 2 \sin 2\theta' \sin 2\theta \cos(\phi' - \phi) + (3 \cos 2\theta' + 1) \sin^2 \theta], \quad (\text{C4})$$

$$F^\times(\theta, \phi, \psi) = -\sin 2\psi [\sin^2 \theta' (\cos 2\theta + 3) \cos[2(\phi' - \phi) - 2 \sin 2\theta' \sin 2\theta \cos(\phi' - \phi) + (3 \cos 2\theta' + 1) \sin^2 \theta]] + \frac{1}{4} [\cos 2\psi (4 \sin^2 \theta' \cos \theta \sin 2(\phi' - \phi) - 4 \sin 2\theta' \sin \theta \sin(\phi' - \phi)]. \quad (\text{C5})$$

Plugging the above results into Eq. (98), yields the corresponding angular efficiency factor

$$F^2 = \int_0^{2\pi} \frac{d\psi}{2\pi} \int \frac{d^2 \hat{\mathbf{n}}}{4\pi} [(F^+)^2 + (F^\times)^2] = \frac{8\pi}{15}. \quad (\text{C6})$$

-
- [1] A. Einstein, Näherungsweise integration der feldgleichungen der gravitation, Sitzungsberichte der Königlich Preußischen Akademie der Wissenschaften , 688 (1916).
- [2] A. Einstein, Über gravitationswellen, Sitzungsber. Preuss. Akad. Wiss. Berlin **154**, 1918 (1918).
- [3] Abbott *et al.*, Observation of gravitational waves from a binary black hole merger, Physical review letters **116**, 061102 (2016).
- [4] G. Agazie, A. Anumalapudi, A. M. Archibald, Z. Arzoumanian, P. T. Baker, B. Bécsy, L. Blecha, A. Brazier, P. R. Brook, S. Burke-Spolaor, *et al.*, The nanograv 15 yr data set: Evidence for a gravitational-wave background, The Astrophysical Journal Letters **951**, L8 (2023).
- [5] N. Aggarwal, O. D. Aguiar, D. Blas, A. Bauswein, G. Cella, S. Clesse, A. M. Cruise, V. Domcke, S. Ellis, D. G. Figueroa, *et al.*, Challenges and opportunities of gravitational wave searches above 10 khz, arXiv preprint arXiv:2501.11723 (2025).
- [6] S. e. a. Abend, Terrestrial very-long-baseline atom interferometry: Workshop summary, AVS Quantum Sci. **6**, 024701 (2024).
- [7] N. Wanwieng, N. Chattrapiban, and A. Watcharangkool, The effects of gravitational waves on a hydrogen atom, Classical and Quantum Gravity **40**, 235004 (2023).
- [8] L. Parker, One-electron atom in curved space-time, Physical Review Letters **44**, 1559 (1980).
- [9] L. Parker and L. O. Pimentel, Gravitational perturbation of the hydrogen spectrum, Physical Review D **25**, 3180 (1982).
- [10] T. Leen, L. Parker, and L. O. Pimentel, Remote quantum mechanical detection of gravitational radiation, General relativity and gravitation **15**, 761 (1983).
- [11] S. Siparov, A two-level atom in the field of a gravitational wave—on the possibility of parametric resonance, Astronomy & Astrophysics **416**, 815 (2004).
- [12] T. Bringmann, V. Domcke, E. Fuchs, and J. Kopp, High-frequency gravitational wave detection via optical frequency modulation, Phys. Rev. D **108**, L061303 (2023).
- [13] Y. Kahn, J. Schütte-Engel, and T. Trickle, Searching for high-frequency gravitational waves with phonons, Phys. Rev. D **109**, 096023 (2024).
- [14] S. Kanno, J. Soda, and A. Taniguchi, Search for high-frequency gravitational waves with rydberg atoms, Eur. Phys. J. C **85** (2025).
- [15] Y. N. Gnedin, A. Mihajlov, L. M. Ignjatović, N. Sakan, V. Srećković, M. Y. Zakharov, N. Bezuglov, and A. Klycharev, Rydberg atoms in astrophysics, New astronomy reviews **53**, 259 (2009).
- [16] P. Roelfsema and W. Goss, High resolution radio recombination line observations, The Astronomy and Astrophysics Review **4**, 161 (1992).

- [17] W. M. Peters, T. J. W. Lazio, T. Clarke, W. Erickson, and N. Kassim, Radio recombination lines at decametre wavelengths—prospects for the future, *Astronomy & Astrophysics* **525**, A128 (2011).
- [18] S. Stepkin, A. Konovalenko, N. G. Kantharia, and N. Udaya Shankar, Radio recombination lines from the largest bound atoms in space, *Monthly Notices of the Royal Astronomical Society* **374**, 852 (2007).
- [19] K. S. Thorne and D. Macdonald, Electrodynamics in curved spacetime: 3+ 1 formulation, *Monthly Notices of the Royal Astronomical Society* **198**, 339 (1982).
- [20] F. K. Manasse and C. W. Misner, Fermi normal coordinates and some basic concepts in differential geometry, *Journal of mathematical physics* **4**, 735 (1963).
- [21] J.-c. Hwang and H. Noh, Definition of electric and magnetic fields in curved spacetime, *Annals of Physics* **454**, 169332 (2023).
- [22] H. Goldstein, C. Poole, J. Safko, and S. R. Addison, *Classical mechanics* (2002).
- [23] I. Beterov, D. Tretyakov, I. Ryabtsev, V. Entin, A. Ekers, and N. Bezuglov, Ionization of rydberg atoms by blackbody radiation, *New Journal of Physics* **11**, 013052 (2009).
- [24] I. Beterov, I. Ryabtsev, D. Tretyakov, and V. Entin, Quasiclassical calculations of blackbody-radiation-induced depopulation rates and effective lifetimes of rydberg n s, n p, and n d alkali-metal atoms with $n \leq 80$, *Physical Review A—Atomic, Molecular, and Optical Physics* **79**, 052504 (2009).
- [25] I. I. Sobel’Man, L. A. Vainshtein, and E. A. Yukov, *Excitation of atoms and broadening of spectral lines*, Vol. 15 (Springer Science & Business Media, 2012).
- [26] M. A. Gordon and R. L. Sorochenko, *Radio Recombination Lines. Their Physics and Astronomical Applications*, Vol. 282 (2002) p. 28.
- [27] N. Šibalić, J. D. Pritchard, C. S. Adams, and K. J. Weatherill, Arc: An open-source library for calculating properties of alkali rydberg atoms, *Computer Physics Communications* **220**, 319 (2017).
- [28] A. Omont, on the theory of collisions of atoms in rydberg states with neutral particles., *J Phys (Paris)* **38**, 1345 (1977).
- [29] N. Thaicharoen, R. Cardman, and G. Raithel, Rydberg electromagnetically induced transparency of ^{85}Rb vapor in a cell with ne buffer gas, *Physical Review Applied* **21**, 064004 (2024).
- [30] M. Sasaki, T. Suyama, T. Tanaka, and S. Yokoyama, Primordial black holes—perspectives in gravitational wave astronomy, *Classical and Quantum Gravity* **35**, 063001 (2018).
- [31] B. Carr and F. Kühnel, Primordial black holes as dark matter: recent developments, *Annual Review of Nuclear and Particle Science* **70**, 355 (2020).
- [32] E. Bagui, S. Clesse, V. De Luca, J. M. Ezquiaga, G. Franciolini, J. García-Bellido, C. Joana, R. K. Jain, S. Kuroyanagi, I. Musco, *et al.*, Primordial black holes and their gravitational-wave signatures, arXiv preprint arXiv:2310.19857 (2023).
- [33] P. M. Morse and H. Feshbach, *Methods of theoretical physics* (Technology Press, 1946).
- [34] S. Kanno, J. Soda, and A. Taniguchi, Search for high-frequency gravitational waves with rydberg atoms, arXiv preprint arXiv:2311.03890 (2023).
- [35] P. Mavrogiannis and C. G. Tsagas, Electromagnetic potentials in curved spacetimes, *Classical and Quantum Gravity* **38**, 235002 (2021).
- [36] N. Aggarwal, O. D. Aguiar, A. Bauswein, G. Cella, S. Clesse, A. M. Cruise, V. Domcke, D. G. Figueroa, A. Geraci, M. Goryachev, *et al.*, Challenges and opportunities of gravitational-wave searches at mhz to ghz frequencies, *Living reviews in relativity* **24**, 1 (2021).
- [37] M. Maggiore, Gravitational wave experiments and early universe cosmology, *Physics Reports* **331**, 283 (2000).